Title page information

Title:

Ocean acidification along the 24.5°N section in the subtropical North Atlantic

Authors:

Elisa F. Guallart [1], Noelia M Fajar[2], Xose Antonio Padín[2], Marcos Vázquez-Rodríguez[2], Eva Calvo[1], Aida F. Ríos[2], Alonso Hernández-Guerra[3], Carles Pelejero[1,4], Fiz F. Pérez[2].

Address:

[1]Institut de Ciències del Mar, Consejo Superior de Investigaciones Científicas, Barcelona, Spain.

[2]Instituto de Investigacións Mariñas, Consejo Superior de Investigaciones Científicas, Vigo, Spain.

[3]Instituto de Oceanografía y Cambio Global (IOCAG), Universidad de Las Palmas de Gran Canaria Las Palmas de Gran Canaria, Spain.

[4]Institució Catalana de Recerca i Estudis Avançats, Barcelona, Spain.

Corresponding author[*]: Elisa F. Guallart

Tel: +34 93 230 9500; Fax: + 34 93 230 95 55

E –mail address: efernandez@icm.csic.es

Abstract

Ocean acidification is directly related to increasing atmospheric CO_2 levels due to human activities and the active role of the global ocean in absorbing part of this anthropogenic CO_2. Here we present an assessment of the pH changes that have occurred along 24.5°N in the subtropical North Atlantic through comparison of pH observations conducted in 1992 and 2011. It reveals an overall decline in pH values in the first 1000 dbar of the water column. The deconvolution of the temporal pH differences into anthropogenic and non-anthropogenic components reveals that natural variability, mostly owed to a decrease in oxygen levels in particular regions of the section, explains the vertical distribution of the larger pH decreases (up to -0.05 pH-units), which are found within the permanent thermocline. The detection of long-term trends in dissolved oxygen in the studied region gains importance for future pH projections, as these changes modulate the anthropogenically-derived acidification. The anthropogenic forcing explains significant acidification deeper than 1000 dbar in the western basin, within the Deep Western Boundary Current.

1. Introduction

Oceans have already absorbed 20-35% of the anthropogenic CO_2 (C_{ant}) emissions [*Khatiwala et al.,* 2009], contributing to mitigate global warming. However, the resulting C_{ant} oceanic invasion affects the chemical balances of the CO_2 system in seawater, raising the amount of total dissolved inorganic carbon in the upper layers, which translates into a decrease in surface ocean pH. On average, the ocean surface waters have already acidified by 0.1 pH units from their pre-industrial levels [*Raven et al.*, 2005]. The oxidation of organic matter also lowers seawater pH by adding CO_2 into the water column. A decrease in seawater acidity can thus also be driven by a larger

accumulation of respired CO_2 as water masses get older, or by a slowdown in the ventilation of these water masses [*Gruber*, 2011]. Ocean acidification has been termed "the other CO_2 problem" [*Doney et al.*, 2009], a phenomenon that affects a number of chemical and biogeochemical properties and processes. The most well-documented implication is the lowering of calcium carbonate ($CaCO_3$) saturation states, which has adverse effects for calcifying organisms, with corals among the most clearly affected marine organisms [*Chan and Connolly*, 2013]. Establishing the rate at which ocean acidification is taking place is important not only to study the fate of marine biota in the face of this global change, but also to understand the future diminishing capacity of the oceans to take up atmospheric CO_2 [*Sabine and Tanhua*, 2010].

In addition to constraining the past variability of seawater pH through the geological record [*Pelejero et al.*, 2010; *Hönisch et al.*, 2012] and forecasting the future from modeling studies [*Resplandy et al.*, 2013], there is still a lot of work to do regarding modern instrumental measurements to document the most recent evolution of ocean pH. A number of studies [*Dore et al.*, 2009; *Byrne et al.*, 2010; *González-Dávila et al.*, 2010; *Vázquez-Rodríguez et al.*, 2012b] have already reported pH changes at decadal scale by means of monitoring at fixed stations and repeating oceanographic sections. The present work assesses the pH changes that have occurred in the Subtropical North Atlantic between 1992 and 2011 from direct observations along a transoceanic line at 24.5°N. These changes, which are studied separately for different water masses, are discussed in the context of the basin-wide circulation.

2. Data and Methods

In July and August 1992, high spatial resolution *in situ* pH measurements were made along the World Ocean Circulation Experiment line A05 at 24.5°N (Figure 1a), between

Las Palmas de Gran Canaria, Spain, and Miami, U.S.A. The pH was measured potentiometrically on 107 stations, with a combined glass electrode associated to a temperature probe [*Perez and Fraga*, 1987], on the National Bureau of Standards scale. The shipboard precision was ± 0.005 pH units [*Ríos and Rosón*, 1996]. The hydrographic section A05 was reoccupied in January–March 2011, within the frame of the Malaspina 2010 expedition [*García-Corral et al.*, 2014]. The pH measurements were obtained on 167 stations using spectrophotometry [*Clayton and Byrne*, 1993], on the total hydrogen ion scale. A correction for dye impurities was applied to the 2011 pH data [*Yao et al.*, 2007]. Measured precision was ± 0.0006. The two pH data sets were converted to the seawater scale and referenced to 25°C, for comparison, using the CO_2sys program [*Pierrot et al.*, 2006] with dissociation constants of *Mehrbach et al.* [1973] and refitted by *Dickson and Millero* [1987]. Total alkalinity (A_T) measurements were obtained in the two cruises by titration of seawater with potentiometric endpoint detection [*Mintrop et al.*, 2000], and the pH–A_T pair was used to derive the complete CO_2 system in each cruise, using the thermodynamic equations reported above. The accuracy of calculated total dissolved inorganic carbon (C_T) was assessed through an analysis of internal consistency, by means of a comparison with calibrated C_T measurements that were also obtained in some of the sampled bottles, in each cruise, in addition to the pH and A_T measurements. The accuracy for calculated C_T data was of ± 2–4 µmol kg^{-1} (n = 12) in 1992 [*Rosón et al.*, 2003] and ± 3.5 µmol kg^{-1} (n = 22) in 2011.

The consistency between the two datasets was investigated by performing a secondary quality control (QC) analysis, following CARbon dioxide IN the Atlantic Ocean (CARINA) procedures [*Tanhua et al.*, 2010]. Measured pH and A_T, calculated C_T, and measured dissolved oxygen (O_2) data were compared in the deep ocean with the

respective data from other cruises at cross-over locations, in order to look for systematic biases. After the analysis, the 1992 pH data were bias adjusted by adding -0.009 pH units and, in order to avoid a new bias in the calculated C_T due to the reduction of pH values without changing A_T, the obtained 1992 A_T correction (- 4 µmol kg^{-1}) was also taken into account (further details in *Guallart et al.* [2013]). By doing this, the original 1992 C_T data, which had shown good consistency with the discrete measured C_T values and a very low offset after QC, were kept almost invariable. No further data adjustments were needed.

Comparison between the 1992 and 2011 data sets was done using bottle data from the stations located within the vertical dashed lines in Fig.1a. For a better comparison, the 1992 and 2011 tracks were made equivalent on latitude first and then the 1992 bottle data grid was interpolated by triangulation into the corresponding depth positions of the 2011 bottle grid using a potential density criterion. The difference in measured pH between 1992 and 2011, ΔpH_m, was calculated as $\Delta pH_m = pH_{m,2011} - pH_{m,1992}$. In order to separate ΔpH_m in its anthropogenic (ΔpH_{ant}) and non-anthropogenic (ΔpH_{Var}, i.e., attributed to natural variability) components, we performed calculations analogous to those reported by *Byrne et al.,* [2010] for a hydrographic line in the North Pacific, maintaining the same nomenclature. We estimated ΔpH_{ant} and ΔpH_{Var} from the observed changes in C_{ant} and natural C_T during the studied period, by means of the thermodynamic equations of the carbonate system. In order to differentiate between the C_{ant} temporal change ($\Delta C_{ant} = C_{ant,2011} - C_{ant,1992}$) and the temporal variability of the natural background of oceanic C_T ($\Delta C_{Var} = C_{Var,2011} - C_{Var,1992}$), the C_{ant} fraction of the C_T estimates in both datasets was isolated using the φC_T^0 method [*Pérez et al.*, 2008; *Vázquez-Rodríguez et al.*, 2009]. This method follows the principles of the ΔC* method [*Gruber et al.*, 1996] given that C_{ant} is calculated from the measured C_T by removing

the contribution of organic matter remineralization, calcium carbonate ($CaCO_3$) dissolution and an estimate of the C_T in the preindustrial atmosphere:

$$C_{ant} = C_T - C_{var}$$
$$= C_T - C_{bio} - \Delta CaCO_3 - C_{T,280} - C_{dis},$$
$$= C_T - AOU/Rc - 0.5\,(PA_T - PA_T°) - C_{T,280} - C_{dis},$$

yet it uses different parameterizations to calculate the air-sea disequilibrium (C_{dis}) and the preformed alkalinity to assess the contribution of $CaCO_3$ dissolution ($\Delta CaCO_3$) on C_T [*Vázquez-Rodríguez et al.*, 2012a]. During the period of study, C_{dis} is assumed not to change significantly. $C_{T,280}$ is the C_T in equilibrium with the preindustrial atmosphere. It is calculated from thermodynamic equations as a function of potential temperature and salinity, preformed alkalinity ($A_T°$), and the corresponding pCO_2 level of 280 ppm. The $A_T°$ correction for $CaCO_3$ dissolution is parameterized from potential A_T (PA_T). Organic matter remineralization has no effect on PA_T, because it already considers the contribution from nitrate and phosphate remineralization, according to Redfield ratios proposed by *Broecker* [1974], but the parameter is subject to alkalinity shifts through the relationship between the dissolution of opal and calcium carbonate [*Vázquez-Rodríguez et al.*, 2012a]. The changes in $CaCO_3$ dissolution can be considered to be negligible over the period of study [*Ilyina et al.*, 2009]. Hence, only the contribution from organic matter remineralization (C_{bio}), which is calculated from apparent oxygen utilization (AOU) according to the oxygen to carbon Redfield ratio (Rc) is a major source of changes in C_{var} at decadal scale, due to changes in the amount of O_2. This method, following the ΔC^* method, uses the Rc ratio from *Anderson and Sarmiento* [1994].

The C_T that these water masses would have had at the end of the 19 years period without the presence of the anthropogenic perturbation ($C_{Var,2011}$) over this timeframe

was estimated from the subtraction of ΔC_{ant} from the C_T values in 2011 ($C_{Var,2011} = C_{T,2011} - \Delta C_{ant}$). The associated pH ($pH_{Var,2011}$) was then calculated using the carbonate system equations with the dissociation constants reported above. $pH_{Var,2011}$ was used to compute the anthropogenic component of the pH change (ΔpH_{ant}) as: $\Delta pH_{ant} = pH_{m,2011} - pH_{Var,2011}$. The natural background component of the pH change was thus computed as $\Delta pH_{Var} = \Delta pH_m - \Delta pH_{ant}$. The uncertainty for ΔpH_m amounts to ±0.0071 and results from error propagation of the uncertainty that can be assigned to each pH data set (i.e., 0.005 pH units) after secondary quality control. The uncertainties for ΔpH_{ant} and ΔpH_{Var} were calculated as the standard deviation of the results found for the respective changes in abyssal waters east of 70°W, as these waters are expected to show C_{ant} levels that fall within the uncertainty of the methodology to estimate C_{ant} [*Brown et al.*, 2010]. These amounted to ± 0.006 and ± 0.005 pH-units, respectively. Following *Sabine et al*, [1999], who found that the error of single C_{ant} estimations (i.e. the method uncertainty) may be a maximum estimate of the random variability in their results because it was larger than the standard deviation of the C_{ant} values below the deepest C_{ant} penetration depth, we also found that the value of ±0.0071 may be the maximum error for ΔpH_m, ΔpH_{ant} and ΔpH_{Var}.

In addition to these calculations, the water column was split into different particular regions following hydrographic criteria: water mass categories and circulation features along the section (see supporting information). The observed changes in pH within these different regions were studied in terms of the observed changes in other chemical properties (Table S2 in the supporting information) to better assess the anthropogenic and non-anthropogenic processes that contribute to them.

3. Results and Discussion

Figures 1b and 1c show the pH distribution along section A05 in 2011, which depict the same basin-wide features as in 1992. The overall pattern consists of high-surface values, higher than 8.05, that decrease rapidly with depth until a pH minimum zone at ~1000 dbar. The prominent pH decrease in the first 1000 dbar is largely associated with remineralization of sinking organic matter by microorganisms [*Millero*, 2007]. The pH minimum (values < 7.65) is found close to the oxygen minimum zone (OMZ) although it is also associated with the influence of aged Antarctic Intermediate Water (AAIW) at depths 800–1100 m depht [*Talley*, 1996]. In the upper ocean, the tilting up of the isolines generates a horizontal gradient in pH in the upper ocean, with pH values becoming lower to the East, with differences of about 0.05 to 0.10 between West and East (Fig. 1b). Below 1200 dbar, the whole section shows relatively homogeneous low pH values of about 7.70–7.73 pH units (Fig. 1c). In the deep ocean, the western basin (>45°W) shows slightly higher pH values between 1500 and 3000 dbar due to the influence of the more recently ventilated Labrador Sea Water (LSW). Closer to the bottom, between 5000 and 6000 dbar, a relative pH minimum identifies the Antarctic Bottom Water.

Figure 2 shows the change in measured pH (ΔpH_m) along the section over the 19 year period (a negative ΔpH_m indicates a lower pH in 2011). Below the seasonal thermocline (red line in the figure [*González-Dávila et al.*, 2010; *Bates et al.*, 2012], the first 1000 dbar of the water column evidence a general decline in pH along the section that ranges between 0 and -0.06 pH units. The larger changes occur mainly in two depth horizons: the subsurface, between ~150 and ~300 dbar (ΔpH_m = -0.03 to -0.06 pH units) and along the whole western basin above the pH minimum zone, between ~400 and ~800 dbar (ΔpH_m = -0.02 to -0.04 pH units). Significant positive differences are observed East of 30°W at intermediate depths. As we discuss below, most of the processes that

explain this vertical profile have sub-annual variability. The mean overall pH difference from 150 to 1000 dbar is -0.023 ± 0.021 pH units. In the deeper ocean, ΔpH_m is greater than -0.01 pH units in the Deep Western Boundary Current (DWBC), West of 70°W, reaching noticeable changes up to -0.02 down to 2000 dbar. The remaining deep ocean does not show pH changes with time distinguishable from zero.

The corresponding ΔpH_{ant} field (Figure 3) indicates the component of ΔpH_m attributed to the atmospheric C_{ant} penetration into the ocean. The ΔpH_{ant} distribution matches the general profile of changes in C_{ant}, which are larger at the surface and progressively lower toward the bottom [*Brown et al.*, 2010]. The greater differences (ΔpH_{ant} of -0.02 to -0.04) extend from the surface until ~ 600 dbar, corresponding to ΔC_{ant} between +10 and 15 µmol kg^{-1} (calculated from our data). When these changes are studied by splitting the section into different density layers, the observed ΔpH_{ant} for the uppermost central layer show mean differences between -0.025 and -0.034 pH-units (Table S2). These values lead to acidification trends for the 1992 – 2011 period, of -0.0014 ± 0.0004 and -0.0018 ± 0.0004 pH units yr^{-1} in the regions next to the western and eastern margins, respectively, which are consistent with those reported for surface waters at BATS (Bermuda Atlantic time-series Study) and ESTOC (European Station for Time series in the Ocean, Canary Islands) Time Series in the Subtropical North Atlantic Gyre [*González-Dávila et al.*, 2010; *Bates et al.*, 2012]. Below 1000 dbar, significant negative ΔpH_{ant} are observed at the edges of the section. The deep acidification in the eastern margin (ΔpH_{ant} ~ -0.02) suggests a confined C_{ant} enrichment (+5 to +10 µmol kg^{-1}) that is presumably due to the influence of the C_{ant}-enriched Mediterranean Water (MW*)* [*Álvarez et al.*, 2005]. The resulting pH trends in the eastern side, in the two layers where MW spreads, are -0.0008 ± 0.0005 and -0.0006 ± 0.0005 pH-units yr^{-1}, which are in agreement with previous results reported in ESTOC [*González-Dávila et*

al., 2010] and in a transect north of 40°N in the eastern North Atlantic Basin [*Vázquez-Rodríguez et al., 2012b]*. West of 70°W, ΔpH_{ant} exhibits a vertically homogeneous structure, from below 1000 dbar to the bottom, of more than -0.011 pH units on average that fully explains the observed ΔpH_m (Figure 2). These changes result from the C_{ant} advected by the DWBC along the deep western margin [*Steinfeldt et al.*, 2009; *Pérez et al.*, 2010]. The acidification signal due to the C_{ant} uptake is even higher from ~ 1000 to ~ 2500 dbar (ΔpH_{ant} = -0.02) due to the spreading of the more recently ventilated core of LSW [*Steinfeldt et al.*, 2009] that moves at these pressure ranges. This upper core shows an acidification trend of -0.0008 ± 0.0005 pH units yr^{-1}, which amounts to half the observed trend for this water mass near the formation region, in the Iceland Basin (-0.0016 ± 0.0002 pH units yr^{-1}) [*Vázquez-Rodríguez et al.*, 2012b]. This can be explained by the dilution of the C_{ant} signal of the water masses within the DWBC while they move southward, owing to mixing with waters from the ocean interior, as already observed in the tropical Atlantic [*Steinfeldt et al.*, 2007]. The extent to which the C_{ant} signal dilutes (denoted by the lower decreasing trend at 24.5°N) is also consistent with the findings of *Van Sebille et al.*[2011], who described a reduction by half of the salinity anomaly signal that was advected through the DWBC, from the source region in the Labrador Sea until 26°N, due to the existence of interior pathways for its transport. The observed full-depth distribution of ΔpH_{ant} along 24.5°N shows a high correlation (r^2 = 0.85) with the independent estimation of this parameter from C_{ant} estimations based in chlorofluorocarbons observations (more details in supporting information).

The ΔpH_{Var} field (Figure 4) is obtained from the difference between ΔpH_m and ΔpH_{ant} fields and indicates changes in C_T due to natural variability in ocean ventilation and respiration processes. In the first 150 dbar, seasonal changes in C_T are driven by biological processes such as primary production and respiration, which encompass

seasonal mixing or stratification events. Below this seasonal thermocline three main structures can be identified as follows:

1. East of 35°W, two cores with values greater than -0.03 pH-units merge through a gradient in ΔpH_{Var} that decreases until ~ 600 dbar, evidencing a coherent structure near the continental margin. These may correspond to the Canary Eddy Corridor, which is a permanent structure in the north-eastern subtropical Atlantic that extends latitudinally from 29°N to 22°N and reaches at least 30°W of longitude [*Sangrà et al.*, 2009]. This corridor recurrently contains long-lived (>3 months) westward propagating mesoscale eddies generated by the Canary Islands whose maximum depths range between 300 and 700 dbar.

2. At deeper depths, a structure with values of -0.01 to -0.03 extends along most of the section with its core between 50°W and 70°W and at ~ 500 to ~ 800 dbar. These changes are located above and partially overlapping the OMZ. They coincide with a region of considerable decrease in O_2 that explain the rise in AOU values by an average of +14 µmol kg^{-1}. These changes may be the cause of the thickening of the OMZ (O_2 below 155 µmol kg^{-1}), since 1992, toward shallower depths.

3. East of 30°W, below 700 dbar, positive ΔpH_{Var} originate from an increase of +10 µmol kg^{-1} in O_2 within the OMZ, without changes in its thickness. The ventilation of the OMZ in the eastern basin is attributable to an enhanced *MW* presence in 2011. This water mass presents a seasonal intrusion in the section with a greater contribution in late winter and spring [*Hernández-Guerra et al.*, 2014]. Hence, this increase in O_2 might be due to latitudinal displacements of waters of southern and Mediterranean origin. On the contrary, the OMZ thickening likely originated from the slow-down in the ventilation of Subpolar Mode Waters [*McCartney and Talley*, 1982] that flow above AAIW,

modulated by shifts in the winds associated to the North Atlantic Oscillation (NAO) [*Bates*, 2012; *Stendardo and Gruber*, 2012]. According to *Johnson and Gruber* [2007], the NAO shift to neutral/negative phase after the mid 1990s (i.e. after the 1992 cruise) caused a lightening of the Subpolar Mode Waters formed afterwards and a reduction of the ventilation of the denser horizons where they spread. This is consistent with our finding of large increases of AOU at the base of the subpolar mode water layer (Fig. 4 and Table S2).

When comparing absolute values of ΔpH_{ant} and ΔpH_{Var} (Figures 3 and 4, respectively), the most relevant feature is that ΔpH_{Var} arises as an important contributor to the observed ΔpH_m (Figure 2) in particular regions of the upper ocean. In the deep ocean, the observed decline in seawater pH within the DWBC is explained only due to changes in C_{ant}. Natural variability of C_T is therefore very likely responsible of the larger decrease in measured pH found below the subsurface within central waters, due to decreases in O_2 (Table S2) that have encompassed the accumulation of C_{ant}. This vertical distribution in negative ΔpH_m matches model simulations of the future evolution of seawater pH over centennial timescales [*Resplandy et al.*, 2013], which project highest-acidification rates in subsurface (mode and intermediate) waters.

The magnitude of the anthropogenic component of the observed pH decrease is expected to increase as atmospheric C_{ant} is gradually absorbed by the ocean [*Byrne et al.*, 2010; *Resplandy et al.*, 2013]. Since C_{ant} changes will always lead to a decreasing ΔpH_m, the anthropogenic forcing becomes more significant for deep and bottom waters because of the higher sensitivity of the more stable deep waters to CO_2 increases, due to their lower alkalinity, temperature, and higher C_T compared with intermediate and mode waters [*Resplandy et al.*, 2013]. In this context, our results suggest that, in the

upper ocean, natural C_T variability is large enough to regionally modulate the seawater pH in two different ways, reinforcing or counteracting the anthropogenically-derived acidification. The reinforcement of ΔpH_{ant} due to negative ΔpH_{Var} is observable close to the OMZ in the western basin, between 400 and 800 dbar and east of 40°W from the subsurface until 600 dbar, causing an even larger reduction of pH. However, in other regions and depths, ΔpH_{Var} counteracts the C_{ant} enrichment, resulting in a net dampening of the acidification signal or even in a pH increase, as observed at intermediate levels of the eastern basin. In addition, the more spatially confined distribution of ΔpH_{Var} results from its modulation by particular changes in O_2 levels.

Similar to the North Pacific, where ventilation was shown to exert a strong control over changes in O_2 [*Byrne et al.*, 2010], in the Subtropical North Atlantic the slow-down in ventilation appears to be the main explanation for the large negative ΔpH_m observed close to the OMZ. These O_2 anomalies operate on decadal timescales, from its relationship to the NAO. Our results also suggest that other important players that modulate O_2 in the studied section include oceanic mesoscale dynamic structures with monthly to seasonal variability such as the Canary Eddy Corridor [*Sangrà et al.*, 2009] and the Frontal Zone between *MW* and Antarctic Intermediate Water [*Zenk et al.*, 1991; *Hernández-Guerra et al.*, 2003]. It is difficult to figure out whether the observed changes in O_2 over longer time frames results from natural variability or from anthropogenic forcing. However, this could be important for long-term pH trends in the studied region given the large interannual to decadal variability in O_2 in the North Atlantic [*Frölicher et al.*, 2009]. In this sense, isolating the human-induced O_2 changes from the mechanisms of ocean O_2 variability that operate on timescales from months to centuries is necessary to better constrain in which regions larger decreases in pH will take place in the future, in the context of anthropogenic climate change.

4. Conclusions

The comparison of seawater pH measurements for the whole water column at 24.5°N in the North Atlantic, between years 1992 and 2011, points to a general decrease in pH values in the first 1000 dbar. Interestingly, highest-acidification rates are exhibited at the subsurface, particularly below the seasonal thermocline. This is caused by a combination of anthropogenic and non-anthropogenic components of similar magnitudes but different representations with depth and longitude along the section. The anthropogenic component is, as expected, more important toward the surface. The nonanthropogenic component, however, displays a much more heterogeneous pattern, with highest decreasing pH rates in specific regions such as that confined below the seasonal thermocline, east of 35°W, and further to the west between 500 and 800 dbar, above the OMZ. This non-anthropogenic component also leads to basification in specific regions along the section. Finally, in the deep western basin there is clear evidence of significant acidification from anthropogenic forcing much deeper than 1000 dbar, virtually extending to the ocean interior, on water masses that move south within the DWBC.

4. Acknowledgements

The 1992 dataset for this paper is available at CDIAC (http://cdiac.ornl.gov); dataset name: 10.3334/CDIAC/OTG.IIM_CSIC_WOCE_A05. The 2011 dataset consists of new data obtained within the frame of the Expedition Malaspina 2010 (http://www.expedicionmalaspina.es) shown here for the first time, which is also available at CDIAC. We acknowledge funding by the Spanish Ministry of Economy and Competitiveness through grants CSD2008-00077 (Circumnavigation Expedition MALASPINA 2010 Project), CTM2009-08849 (ACDC Project) and CTM2012-32017

(MANIFEST Project), and from the Seventh Framework Programme FP7 CARBOCHANGE (grant agreement 264879). E.F. Guallart was funded by CSIC through a JAE-Pre grant. We thank the editor and two anonymous reviewers for their critical reading and constructive comments.

Álvarez, M., F. F. Pérez, D. R. Shoosmith, and H. L. Bryden (2005), Unaccounted role of Mediterranean Water in the drawdown of anthropogenic carbon, *J. Geophys. Res.*, *110*, C09S03, doi:10.1029/2004JC002633.

Anderson, L. A., and J. L. Sarmiento (1994), Redfield ratios of remineralization determined by nutrient data analysis, *Global Biogeochem. Cycles*, *8*(1), 65–80, doi:10.1029/93GB03318.

Bates, N. R. (2012), Multi-decadal uptake of carbon dioxide into subtropical mode water of the North Atlantic Ocean, *Biogeosciences*, *9*(7), 2649–2659.

Bates, N. R., M. H. P. Best, K. Neely, R. Garley, A. G. Dickson, and R. J. Johnson (2012), Detecting anthropogenic carbon dioxide uptake and ocean acidification in the North Atlantic Ocean, *Biogeosciences*, *9*(1), 2509–2522.

Broecker, W. S. (1974), "NO" a conservative water mass tracer, *Earth Planet. Sci. Lett.*, *23*, 8761–8776.

Brown, P. J., D. C. E. Bakker, U. Schuster, and A. J. Watson (2010), Anthropogenic carbon accumulation in the subtropical North Atlantic, *J. Geophys. Res.*, *115*, C04016, doi:10.1029/2008JC005043.

Byrne, R. H., S. Mecking, R. A. Feely, and X. Liu (2010), Direct observations of basin-wide acidification of the North Pacific Ocean, *Geophys. Res. Lett.*, *37*, L02601, doi:10.1029/2009GL040999.

Chan, N. C. S., and S. R. Connolly (2013), Sensitivity of coral calcification to ocean acidification: A meta-analysis, *Global Change Biol.*, *19*(1), 282–290.

Clayton, T. D., and R. H. Byrne (1993), Spectrophotometric seawater pH measurements: Total hydrogen ion concentration scale calibration of m-cresol purple and at-sea results, *Deep Sea Res., Part I, 40*(10), 2115–2129.

Dickson, A. G., and F. J. Millero (1987), A comparison of the equilibrium constants for the dissociation of carbonic acid in seawater media, Deep Sea Res., Part A, 34(10), 1733–1743.

Doney, S. C., V. J. Fabry, R. A. Feely, and J. A. Kleypas (2009), Ocean acidification: The other CO_2 problem, *Annu. Rev. Mar. Sci., 1*(1), 169–192, doi:10.1146/annurev.marine.010908.163834.

Dore, J. E., R. Lukas, D. W. Sadler, M. J. Church, and D. M. Karl (2009), Physical and biogeochemical modulation of ocean acidification in the central North Pacific, *Proc. Natl. Acad. Sci. U.S.A., 106*(30), 12,235–12,240.

Frölicher, T. L., F. Joos, G. K. Plattner, M. Steinacher, and S. C. Doney (2009), Natural variability and anthropogenic trends in oceanic oxygen in a coupled carbon cycle-climate model ensemble, *Global Biogeochem. Cycles, 23*, GB1003, doi:10.1029/2008GB003316.

García-Corral, L. S., E. Barber, A. Regaudie-de-Gioux, S. Sal, J. M. Holding, S. Agustí, N. Navarro, P. Serret, P. Mozetič, and C. M. Duarte (2014), Temperature dependence of planktonic metabolism in the subtropical North Atlantic Ocean, *Biogeosciences, 11*(16), 4529–4540.

González-Dávila, M., J. M. Santana-Casiano, M. J. Rueda, and O. Llinás (2010), The water column distribution of carbonate system variables at the ESTOC site from 1995 to 2004, *Biogeosciences, 7,* 3067–3081.

Gruber, N. (2011), Warming up, turning sour, losing breath: Ocean biogeochemistry under global change, *Philos. Trans. R. Soc. A, 369*(1943), 1980–1996.

Gruber, N., J. L. Sarmiento, and T. F. Stocker (1996), An improved method for detecting anthropogenic CO_2 in the oceans, *Global Biogeochem. Cycles, 10*(4), 809–837, doi:10.1029/96GB01608.

Guallart, E. F., F. F. Pérez, G. Rosón, and A. F. Ríos (2013), High spatial resolution alkalinity and pH measurements by IIM-CSIC group along 24.5°N during the R/V Hespérides WOCE section A05 cruise, Rep., Instituto de Investifaciones Marinas, Consejo Superior de Investigaciones Científicas. [Available at http://digital.csic.es/handle/10261/93331].

Hernández-Guerra, A., E. Fraile-Nuez, R. Borges, F. López-Laatzen, P. Vélez-Belchí, G. Parrilla, and T. J. Müller (2003), Transport variability in the Lanzarote passage (eastern boundary current of the North Atlantic subtropical Gyre), *Deep Sea Res., Part I, 50*(2), 189–200.

Hernández-Guerra, A., J. L. Pelegrí, E. Fraile-Nuez, V. Benítez-Barrios, M. Emelianov, M. D. Pérez-Hernández, and P. Vélez-Belchí (2014), Meridional overturning transports at 7.5 N and 24.5 N in the Atlantic Ocean during 1992–93 and 2010–11, *Prog. Oceanogr., 128,* 98–114.

Hönisch, B., et al. (2012), The geological record of ocean acidification, *Science, 335*(6072), 1058–1063.

Ilyina, T., R. E. Zeebe, E. Maier-Reimer, and C. Heinze (2009), Early detection of ocean acidification effects on marine calcification, *Global Biogeochem. Cycles, 23*, GB1008, doi:10.1029/2008GB003278.

Johnson, G. C., and N. Gruber (2007), Decadal water mass variations along 20°W in the Northeastern Atlantic Ocean, *Prog. Oceanogr., 73*(3–4), 277–295.

Khatiwala, S., F. Primeau, and T. Hall (2009), Reconstruction of the history of anthropogenic CO_2 concentrations in the ocean, *Nature, 462*(7271), 346–349.

McCartney, M. S., and L. D. Talley (1982), The subpolar mode water of the North Atlantic Ocean, J. *Phys. Oceanogr., 12*(11), 1169–1188.

Mehrbach, C., C. H. Culberson, J. E. Hawley, and R. M. Pytkowicz (1973), Measurement of the apparent dissociation constants of carbonic acid in seawater at atmospheric pressure, *Limnol. Oceanogr., 18*(6), 897–907.

Millero, F. J. (2007), The marine inorganic carbon cycle, *Chem. Rev., 107*(2), 308–341.

Mintrop, L., F. F. Pérez, M. González-Dávila, J. M. Santana-Casiano, and A. Körtzinger (2000), Alkalinity determination by potentiometry: Intercalibration using three different methods, *Cienc. Mar., 26*(1), 23–27. [Available at http://hdl.handle.net/10261/25136.]

Pelejero, C., E. Calvo, and O. Hoegh-Guldberg (2010), Paleo-perspectives on ocean acidification, *Trends Ecol. Evol., 25*(6), 332–344.

Perez, F. F., and F. Fraga (1987), The pH measurements in seawater on the NBS scale, *Mar. Chem.*, *21*(4), 315–327.

Pérez, F. F., M. Vázquez-Rodríguez, E. Louarn, X. A. Padín, H. Mercier, and A. F. Ríos (2008), Temporal variability of the anthropogenic CO_2 storage in the Irminger Sea, *Biogeosciences*, *5*(6), 1669–1679.

Pérez, F. F., M. Vázquez-Rodríguez, H. Mercier, A. Velo, P. Lherminier, and A. F. Ríos (2010), Trends of anthropogenic CO2 storage in North Atlantic water masses, *Biogeosciences*, *7*(5), 1789–1807.

Pierrot, D., E. Lewis, and D. Wallace (2006), MS Excel Program Developed for CO_2 System Calculations, ORNL/CDIAC-105a, edited, Carbon Dioxide Information Analysis Center, Oak Ridge National Laboratory, US Department of Energy, Oak Ridge, Tenn.

Raven, J., K. Caldeira, H. Elderfield, O. Hoegh-Guldberg, P. Liss, U. Riebesell, J. Shepherd, C. Turley, and A. Watson (2005), *Ocean Acidification Due to Increasing Atmospheric Carbon Dioxide*, Royal Society, London.

Resplandy, L., L. Bopp, J. C. Orr, and J. P. Dunne (2013), Role of mode and intermediate waters in future ocean acidification: Analysis of CMIP5 models, *Geophys. Res. Lett.*, *40*, 3091–3095, doi:10.1002/grl.50414.

Ríos, A. F., and G. Rosón (1996), pH and alkalinity measurements, *Rep.*, pp. 64–73, Lab. de Phys. des Océans, Brest, France.

Rosón, G., A. F. Ríos, F. F. Pérez, A. Lavín, and H. L. Bryden (2003), Carbon distribution, fluxes, and budgets in the subtropical North Atlantic Ocean (24.5°N), J. *Geophys. Res., 108*(C5), 3144, doi:10.1029/1999JC000047.

Sabine, C. L., and T. Tanhua (2010), Estimation of anthropogenic CO_2 inventories in the ocean, *Annu. Rev. Mar. Sci., 2*(1), 175–198.

Sabine, C. L., R. M. Key, K. M. Johnson, F. J. Millero, A. Poisson, J. L. Sarmiento, D. W. R. Wallace, and C. D. Winn (1999), Anthropogenic CO_2 inventory of the Indian Ocean, *Global Biogeochem. Cycles, 13*(1), 179–198, doi:10.1029/1998GB900022.

Sangrà, P., A. Pascual, Á. Rodríguez-Santana, F. Machín, E. Mason, J. C. McWilliams, J. L. Pelegrí, C. Dong, A. Rubio, and J. Arístegui (2009), The Canary Eddy Corridor: A major pathway for long-lived eddies in the subtropical North Atlantic, *Deep Sea Res., Part I, 56*(12), 2100–2114.

Steinfeldt, R., M. Rhein, and M. Walter (2007), NADW transformation at the western boundary between 66°W/20°N and 60°W/10°N, *Deep Sea Res., Part I, 54*, 835–855.

Steinfeldt, R., M. Rhein, J. L. Bullister, and T. Tanhua (2009), Inventory changes in anthropogenic carbon from 1997–2003 in the Atlantic Ocean between 20°S and 65°N, *Global Biogeochem. Cycles, 23*, GB3010, doi:10.1029/2008GB003311.

Stendardo, I., and N. Gruber (2012), Oxygen trends over five decades in the North Atlantic, *J. Geophys. Res., 117*, C11004, doi:10.1029/2012JC007909.

Talley, L. D. (1996), Antarctic intermediate water in the South Atlantic, in *The South Atlantic*, edited, pp. 219–238, Springer, Berlin.

Tanhua, T., S. van Heuven, R. M. Key, A. Velo, A. Olsen, and C. Schirnick (2010), Quality control procedures and methods of the CARINA database, *Earth Syst. Sci. Data*, *2*, 35–49.

van Sebille, E., M. O. Baringer,W. E. Johns, C. S. Meinen, L. M. Beal, M. F. de Jong, and H. M. van Aken (2011), Propagation pathways of classical Labrador Sea water from its source region to 26°N, *J. Geophys. Res.*, *116*, C12027, doi:10.1029/2011JC007171.

Vázquez-Rodríguez, M., F. Touratier, C. Lo Monaco, D. W. Waugh, X. A. Padin, R. G. J. Bellerby, C. Goyet, N. Metzl, A. F. Ríos, and F. F. Pérez (2009), Anthropogenic carbon distributions in the Atlantic Ocean: Data-based estimates from the Arctic to the Antarctic, *Biogeosciences*, *6*(3), 439–451.

Vázquez-Rodríguez, M., X. A. Padin, P. C. Pardo, A. F. Ríos, and F. F. Pérez (2012a), The subsurface layer reference to calculate preformed alkalinity and air-sea CO_2 disequilibrium in the Atlantic Ocean, *J. Mar. Syst.*, *94*, 52–63.

Vázquez-Rodríguez, M., F. F. Pérez, A. Velo, A. F. Ríos, and H. Mercier (2012b), Observed acidification trends in North Atlantic water masses, *Biogeosciences*, *9*(12), 5217–5230.

Yao, W., X. Liu, and R. H. Byrne (2007), Impurities in indicators used for spectrophotometric seawater pH measurements: Assessment and remedies, *Mar. Chem.*, *107*(2), 167–172.

Zenk, W., B. Klein, and M. Schroder (1991), Cape Verde Frontal Zone, *Deep Sea Res., Part A*, *38*(Supplement 1), S505–S530.

Figure 1. a) Sampling stations for pH measurements along the hydrographic section A05 in the subtropical North Atlantic, in 1992 (red) and in 2011 (white). (b and c) The distributions of reference pH (25°C) on the seawater scale (pH_{sws}) in 2011 for the upper (first 1000 dbar) and the deep ocean, respectively. The reported pH values correspond to longitude coordinates within the vertical dashed lines in Figure 1a.

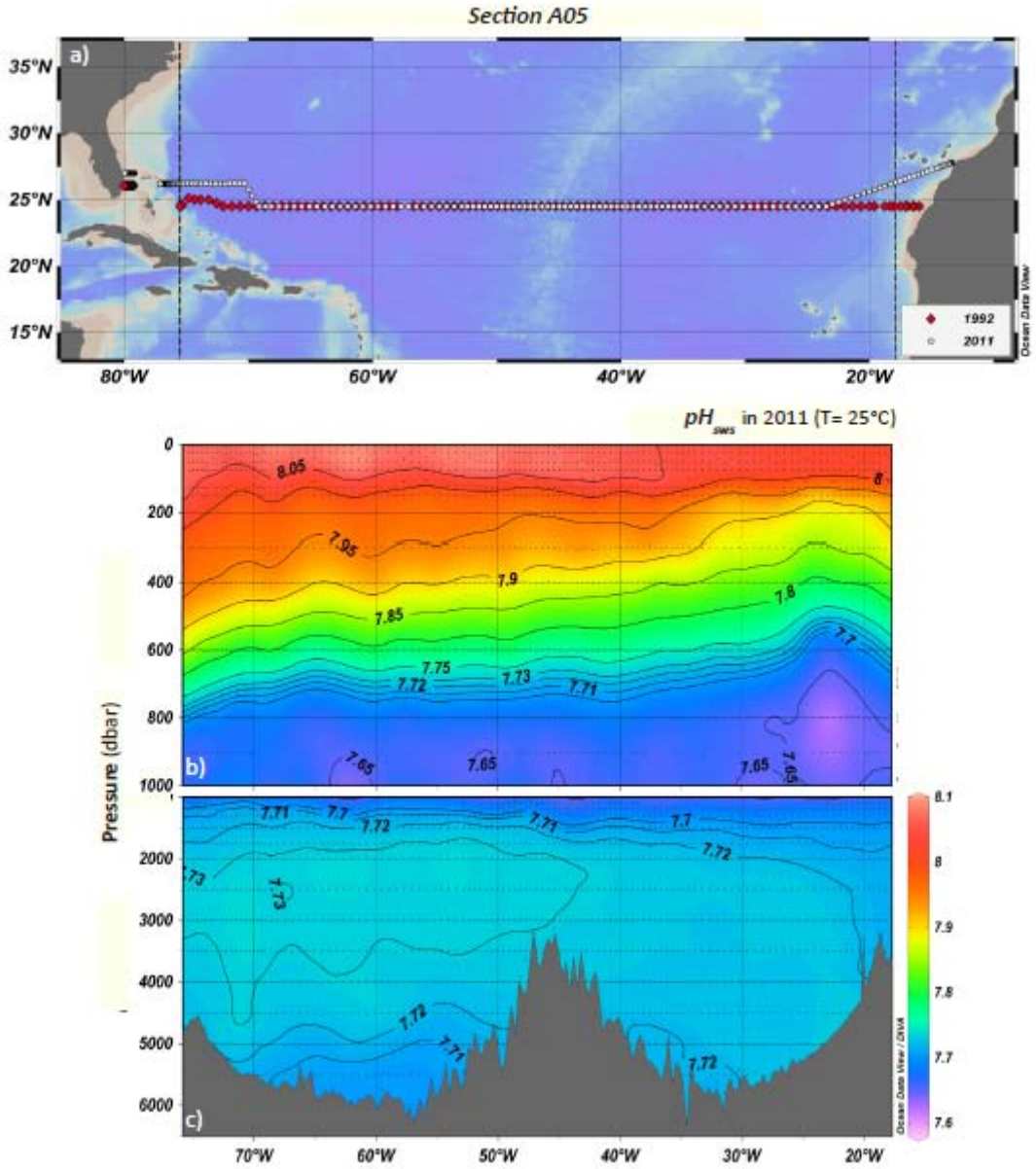

Figure 2. Change in seawater pH, ΔpH_m, along the section A05 between 1992 and 2011. The red line shows the location of the seasonal thermocline at these latitudes [*González-Dávila et al.*, 2010; *Bates et al.*, 2012].

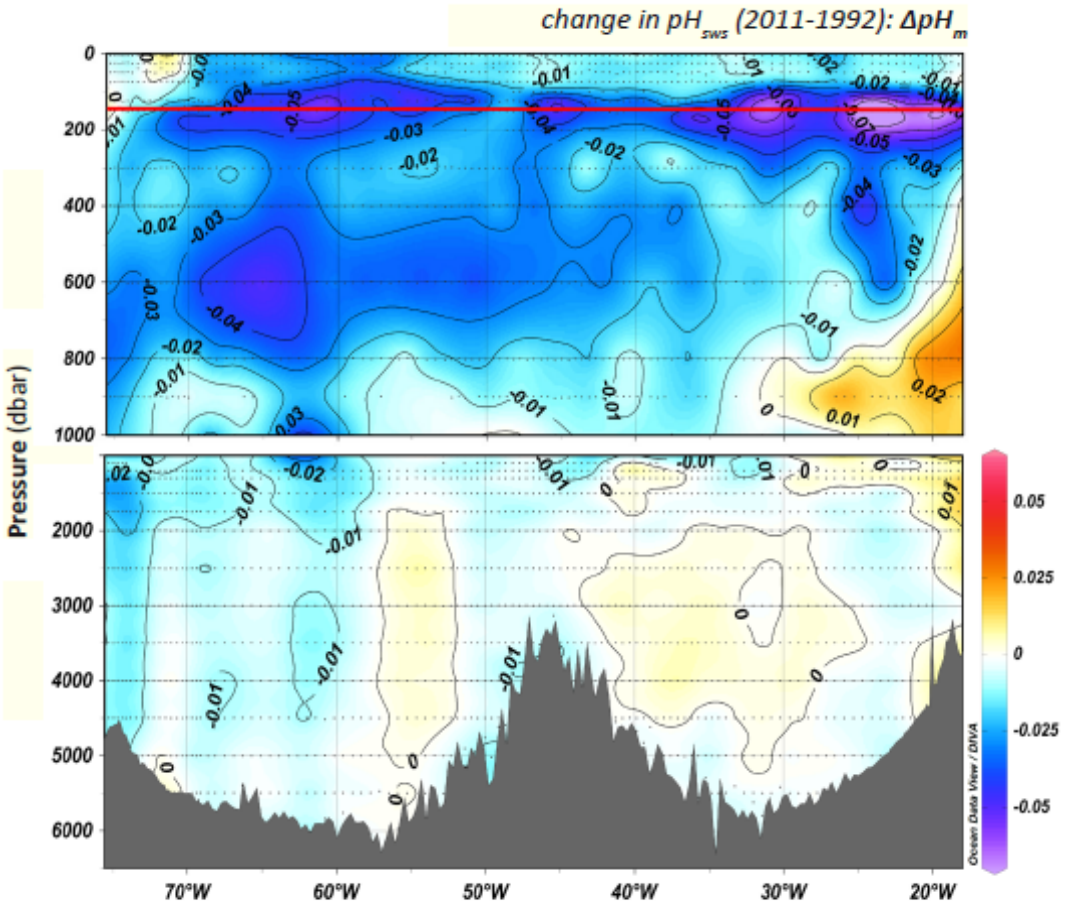

Figure 3. Change in seawater pH attributed to the C_{ant} uptake by the surface ocean between 1992 and 2011, ΔpH_{ant}, along the A05 section. Red line as in Figure 2.

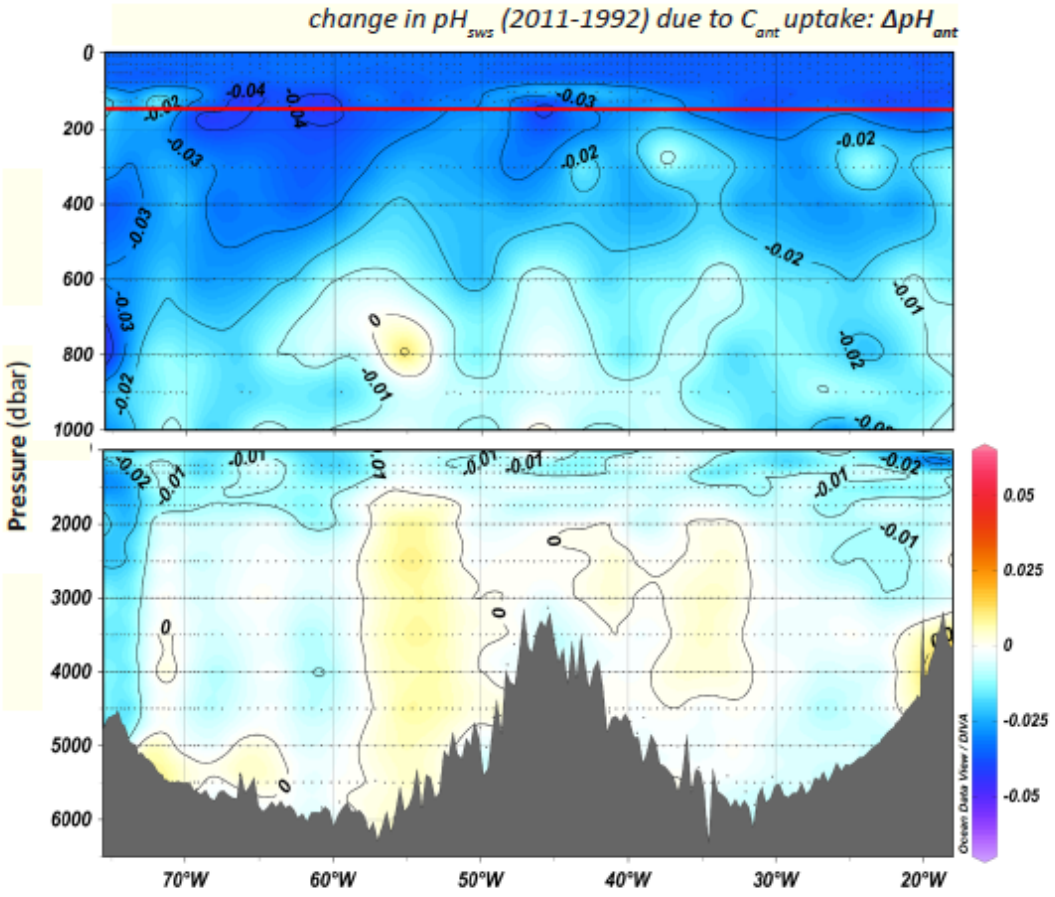

Figure 4. Change in seawater pH attributed to changes in the natural C_T background between 1992 and 2011, ΔpH_{Var}, along the A05 section. Thick red line as in Figure 2. The three thin dark red lines below depict the bottom isopycnal boundaries (σ_0 = 26.7; σ_0 = 27.2; σ_0 = 27.6) chosen to delimit, respectively, the upper (subtropical origin) and lower (subpolar origin) limbs of Central Water: uNACW and lNACW and Antarctic Intermediate Water (AAIW) (see supporting information). The blue lines depict the OMZ (i.e., oxygen levels under 155 µmol kg^{-1}) horizon in 1992 (dashed line) and in 2011 (dashed-dotted line).

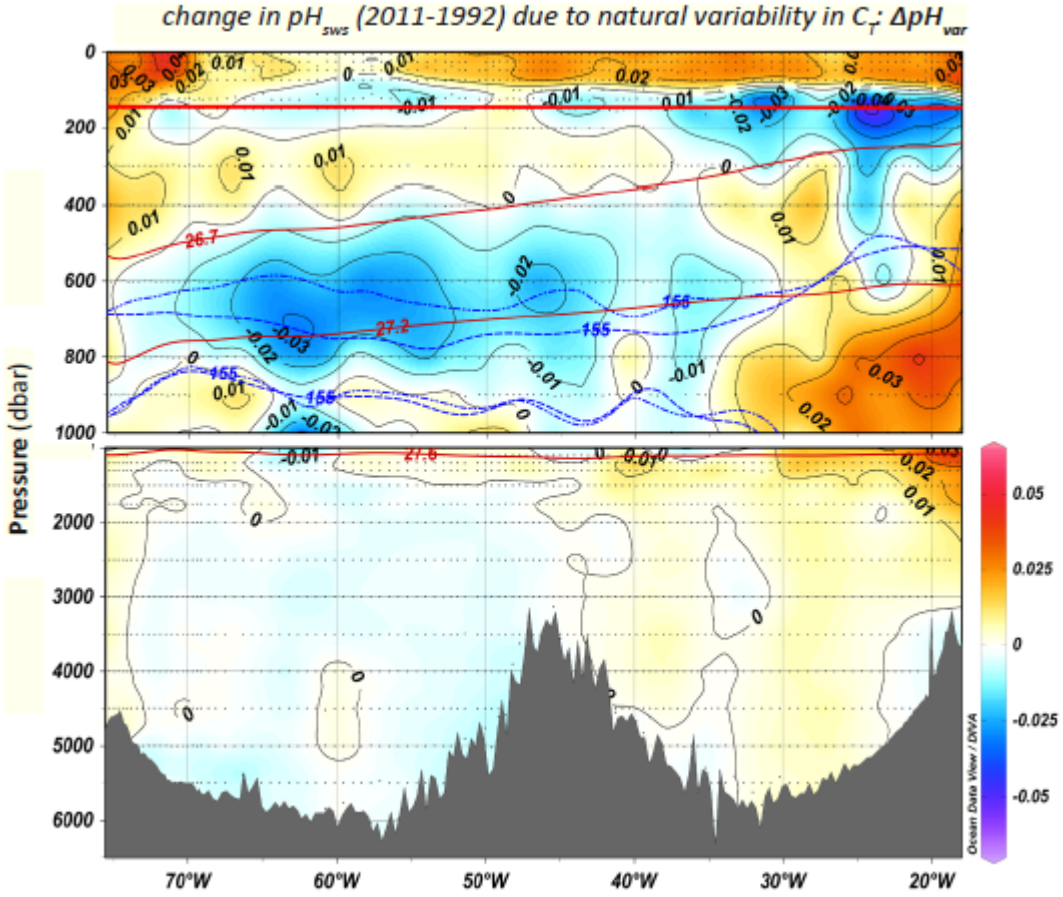

Supporting Information

Methods

Figures

Tables

A. Division of the datasets in density layers and zonal regions

In order to better assess the processes behind the observed changes in the chemical properties between 1992 and 2011, the water column was divided in six density categories following *Talley et al.,* [2011]. The main water masses present in the Subtropical North Atlantic were identified as: upper North Atlantic Central Water (*uNACW)*, lower North Atlantic Central Water (*lNACW*), Antarctic Intermediate Water (*AAIW*), upper North Atlantic Deep Water (*uNADW*), lower North Atlantic Deep Water (l*NADW*) and Antarctic Bottom Water (*AABW*). The dataset was further divided longitudinally taking into account the separation into the two main basins (western/eastern) and a more refined subdivision of these to isolate the spreading regions of the Deep Western Boundary Current and the Mediterranean Water, which are situated at the western and eastern margins, respectively. Table S1 sums up the corresponding isopycnals and geographic coordinates taken into account to split the

section A05 in different regions. A number of 22 subdivisions of the section were obtained (Figure S1).

Supplementary Table S1. Isopycnal boundaries and geographic coordinates considered to split the section A05 in different subdivisions following hydrographic criteria.

WATER MASS	Density layer (kgm^{-3})	**REGION**	Longitude (°)
uNACW	σ_0<26.7	***Region 1***	80°W to 70°W
lNACW	26.7<σ_0<27.2	***Region 2***	70°W to 45°W
AAIW	27.2<σ_0<27.6	***Region 3***	45°W to 30°W
uNADW	σ_0>27.6 and σ_2<37	***Region 4***	30°W to 10°W
lNADW	σ_2>37 and σ_4<45.9		
AABW	σ_4<45.9		

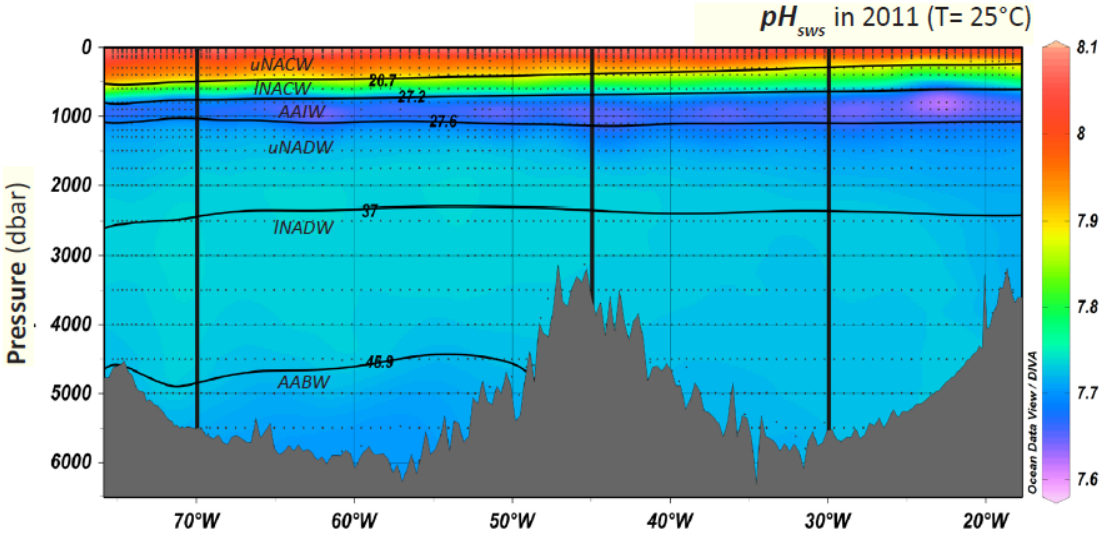

Supplementary Figure S1. Hydrographic regions in which the section A05 was divided, over the pH distribution of the 2011 cruise. The boundaries of the different subdivisions follow details given in Table S1.

B. <u>Average parameters per layer and region</u>

The average and standard deviation (SD) of the mean of the following parameters was computed with data within each of the 22 subdivisions: Measured pH in the seawater scale and referred to 25°C (*pHsws25*) in 2011 and 1992; Change in measured pH (2011-1992, ΔpH_m), further decomposed into the respective anthropogenic (ΔpH_{ant}) and non-anthropogenic (ΔpH_{Var}) contributions; Change in Apparent Oxygen Utilization, *AOU* (ΔAOU); Change in C_{ant} using the φC_T^0 method ($\Delta\varphi C_T^0$) and change in C_{ant} using the TTD method (ΔTTD, further details in section C).

Only bottle data between 75.27°W and 18.27°W were considered for the computations, in order to calculate the changes between the two datasets with data closer than 2 degrees of latitude. Data of the first 150 dbar were also rejected to avoid seasonal variability in the above parameters. Mean values ± uncertainty (SD) are shown in Table S2.

Supplementary Table S2. Mean values ± standard deviation (x ± SD) for measured pH (*pHsws25*) in 2011 and 1992, change in measured pH (ΔpH_m), anthropogenic (ΔpH_{ant}) and non-anthropogenic (ΔpH_{Var}) contributions to ΔpH_m, change in Apparent Oxygen Utilization (ΔAOU) in µmol/kg, change in C_{ant} using the φC_T^0 ($\Delta\varphi C_T^0$) and TTD (ΔTTD) methods in µmols·kg^{-1}, within each given subdivision. By dividing mean ΔpH_{ant} in regions 1 and 4 in uNACW, region 4 in AAIW and uNADW and region 1 in uNADW, the following pH decreasing trends (pH-units yr^{-1}) due to C_{ant} uptake are obtained, respectively: -0.0014±0.0004, -0.0018±0.0004, -0.0008±0.0004, -0.0006±0.0005 and -0.0008±0.0005. Bold numbers indicate statistical significance (*t* test < 0.05). Column *N* indicates the number of values within each subdivision.

		pHsws25 2011	*pHsws25 1992*	*N*	ΔpH_m (2011-1992)	p-value	ΔpH_{ant} (2011-1992)	p-value	ΔpH_{Var} (2011-1992)	p-value	ΔAOU (2011-1992)	$\Delta \varphi CT^0$ (2011-1992)	ΔTTD (2011-1992)
uNACW	**1**	7.972±0.036	7.992±0.033	48	**-0.020±0.015**	0.000	**-0.028±0.008**	0.000	**0.008±0.012**	0.000	**-3.4±9.8**	**16.2±4.8**	**20.9±1.6**
	2	7.950±0.034	7.980±0.040	139	**-0.030±0.014**	0.000	**-0.032±0.008**	0.000	0.002±0.009	0.048	**2.5±8.2**	**18.4±5.4**	**21.3±1.7**
	3	7.953±0.038	7.984±0.046	67	**-0.031±0.023**	0.000	**-0.025±0.015**	0.000	**-0.006±0.012**	0.000	**8.6±10.4**	**14.5±9.0**	**21.7±1.7**
	4	7.922±0.030	7.984±0.025	29	**-0.062±0.028**	0.000	**-0.034±0.008**	0.000	**-0.028±0.027**	0.000	**28.1±18.7**	**19.3±4.6**	**21.9±0.8**
lNACW	**1**	7.794±0.050	7.824±0.051	21	**-0.029±0.007**	0.000	**-0.027±0.010**	0.000	-0.003±0.007	0.080	**3.7±4.7**	**12.4±4.2**	**13.3±2.4**
	2	7.792±0.039	7.830±0.038	56	**-0.038±0.010**	0.000	**-0.018±0.009**	0.000	**-0.019±0.010**	0.000	**14.2±6.0**	**8.5±4.3**	**14.3±2.0**
	3	7.812±0.055	7.837±0.057	67	**-0.025±0.011**	0.000	**-0.018±0.008**	0.000	**-0.006±0.011**	0.000	**8.0±7.6**	**8.9±4.1**	**15.4±2.7**
	4	7.797±0.065	7.816±0.068	63	**-0.019±0.024**	0.000	**-0.020±0.012**	0.000	0.001±0.026	0.764	2.8±18.1	**9.5±5.7**	**15.9±2.5**
AAIW	**1**	7.674±0.011	7.691±0.013	42	**-0.017±0.009**	0.000	**-0.018±0.007**	0.000	0.000±0.008	0.201	0.7±4.8	**7.1±3.0**	**6.8±0.9**
	2	7.666±0.017	7.681±0.017	118	**-0.015±0.015**	0.000	**-0.008±0.011**	0.000	**-0.006±0.015**	0.000	**2.4±6.9**	**3.4±4.4**	**5.3±1.2**
	3	7.664±0.012	7.676±0.013	93	**-0.012±0.009**	0.000	**-0.010±0.006**	0.000	-0.002±0.011	0.187	**1.4±5.2**	**4.1±2.3**	**4.5±1.3**
	4	7.646±0.019	7.638±0.019	66	**0.008±0.021**	0.000	**-0.014±0.008**	0.000	**0.025±0.018**	0.000	**-8.7±8.5**	**5.7±3.2**	**4.8±1.9**
uNADW	**1**	7.718±0.011	7.732±0.013	99	**-0.015±0.008**	0.000	**-0.016±0.009**	0.000	**0.001±0.003**	0.000	**-0.5±1.6**	**6.6±3.6**	**7.8±1.4**
	2	7.716±0.015	7.725±0.015	238	**-0.008±0.007**	0.000	**-0.008±0.007**	0.000	-0.001±0.005	0.089	**-1.1±2.9**	**3.2±3.0**	**4.8±1.6**
	3	7.704±0.019	7.706±0.019	160	**-0.003±0.007**	0.000	**-0.007±0.007**	0.000	**0.004±0.006**	0.000	-0.3±2.9	**2.9±2.7**	**2.7±0.4**
	4	7.698±0.016	7.697±0.018	121	0.001±0.008	0.143	**-0.012±0.009**	0.000	**0.013±0.011**	0.000	**-2.8±3.7**	**5.1±3.7**	**2.8±1.0**
lNADW	**1**	7.730±0.004	7.738±0.006	74	**-0.008±0.007**	0.000	**-0.008±0.009**	0.000	0.000±0.004	0.605	**1.0±2.2**	**3.2±3.9**	**4.8±0.6**
	2	7.729±0.004	7.735±0.006	209	**-0.005±0.006**	0.000	**-0.002±0.006**	0.000	**-0.003±0.003**	0.000	**1.1±2.4**	**0.7±2.7**	**2.6±0.8**
	3	7.724±0.004	7.724±0.006	203	0.000±0.006	0.542	**-0.001±0.006**	0.032	**0.001±0.003**	0.011	**2.1±1.9**	**0.4±2.4**	**1.6±0.3**
	4	7.723±0.005	7.726±0.006	117	**-0.002±0.006**	0.000	**-0.006±0.006**	0.000	**0.003±0.003**	0.000	**-0.5±3.0**	**2.4±2.7**	**1.5±0.2**
AABW	**1**	7.719±0.006	7.725±0.010	18	-0.004±0.008	0.061	-0.001±0.012	0.614	-0.003±0.006	0.082	1.0±2.8	0.7±5.0	**3.0±0.8**
	2	7.711±0.007	7.715±0.008	112	**-0.004±0.007**	0.000	0.000±0.006	0.506	**-0.005±0.004**	0.000	**2.4±2.1**	-0.2±2.7	**2.6±1.4**

C. Change in C_{ant} TTD

C_{ant} needs to be derived by indirect techniques from *in-situ* observations. The φC_T^0 method [*Pérez et al.*, 2008; *Vázquez-Rodríguez et al.*, 2009] for C_{ant} estimation builds on back-calculation principles that try to separate the C_{ant} signal from the background CO_2 distribution [*Brewer*, 1978; *Chen and Millero*, 1979]. It is performed by removing an estimate of the preindustrial preformed C_T and by correcting the C_T values for changes due to the biological activity. Together with a number of other close methodologies (ΔC^*(Gruber et al., 1996), ΔC_T^0 [*Kortzinger et al.*, 1998], TrOCA [*Touratier and Goyet*, 2004; *Touratier et al.*, 2007]), the φC_T^0 method relies on observations of the parameters of the CO_2 system to estimate C_{ant}. However, there exist other approaches to estimate C_{ant} without using CO_2 measurements, which depend on tracer observations. Due to the availability of CFCs measurements in the 1992 occupation (W. Smethie, Principal Investigator, Lamont-Doherty Earth Observatory, http://cdiac.ornl.gov/), C_{ant} concentrations were also estimated using the TTD method [*Waugh et al.*, 2006]. Thus, CFCs observations are used as a proxy of C_{ant} since they serve to constrain the time elapsed since a water parcel was last in contact with the surface to describe how the ocean circulation connects the surface with the interior ocean concentrations, by means of particular functions called Transient Time Distributions (TTD) [*Waugh et al.*, 2004; *Waugh et al.*, 2006]. CFC-12 data were used to constrain the TTD functions. The CFC-12's partial pressures at interior locations were calculated by using the solubility functions determined by *Warner and Weiss* [1985] assuming a time-invariant initial saturation at 100% for mode waters, at 85% for intermediate waters and at 65% for deep and bottom waters.

Since the assumption of the TTD transport is steady, the temporal change in the TTD estimates (from 1992 until 2011) can be approximated considering a steadier behavior

of the C_{ant} concentrations distributions in the region of interest [*Tanhua et al.*, 2006; *Tanhua et al.*, 2007; *Steinfeldt et al.*, 2009]. The change in the C_{ant} concentrations by the end of the studied period (2011) can be thus computed assuming an annual increment of 1.69% [*Steinfeldt et al.*, 2009] of the C_{ant} estimations for a given year (cruise) and considering the lapse in time from then until 2011.

Following the average ΔpH_{ant} values reported in Table S2, the estimation of the anthropogenic component of ΔpH_m between 1992 and 2011 was evaluated, through linear regression, in terms of the average ΔpH_{ant}-TTD that resulted from the change in the obtained C_{ant}-TTD estimates during the same period (Figure S2). The linear regression between the two estimations ($\Delta pH_{ant} = 0.745\Delta pH_{ant}\text{-TTD} - 0.0004$) showed a coefficient of determination (r^2) of 0.85. This high value attests to the robustness of the C_{ant} values used to estimate ΔpH_{ant} through the φC_T^0 method, since the estimated ΔpH_{ant} strongly correlates with the corresponding independent estimations of ΔpH_{ant}-*TTD* that do not rely on CO_2 measurements. There are some values, corresponding to the two central layers, that slightly deviate from the $\Delta pH_{ant} = \Delta pH_{ant}$-TTD regression line, which may be due the fact that the C_{ant}-TTD values were somewhat high [*Khatiwala et al.*, 2013] compared to the C_{ant}-φC_T^0 values in the uppermost layer for the 1992 cruise and also due to the assumption of overall steady accumulation. These two factors may lead to greater C_{ant}-TTD and, thus, to greater ΔpH_{ant}-TTD changes for these two layers at the end of the studied period. However, the error of the y-intercept (b = -0.0004) of the linear fit amounts to ± 0.0016, which also suggests that the residuals fall within the uncertainty of the pH changes and that both ΔpH_{ant} and ΔpH_{ant}-TTD estimates are thus consistent between them. The uncertainty related to the linear fit (i.e. the error related to the calculation of the ΔpH_{ant} term by using this linear equation) equals ± 0.004. Taking into account that the two estimations are independent between

them, this error can be considered as the uncertainty related to the estimation of the anthropogenic component of ΔpH_m, since the linear equation includes variability not only due to the uncertainty of the measurements but to the actual variability, of unknown origin, in this parameter. This value is lower than the uncertainty of ± 0.0071 considered in the main manuscript, so we have taken this latter value also in a conservative way as the maximum error for ΔpH_m, ΔpH_{ant} and $\Delta pH_{Var.}$

Supplementary Figure S2. Linear correlation (in blue) between the change in measured pH due to the anthropogenic forcing between 1992 and 2011 obtained by using the φC_T^0 method (ΔpH_{ant}), and the same parameter obtained by using CFC measurements and the TTD method (ΔpH_{ant}-TTD). The coefficient of determination (r^2) was 0.85. The linear correlation corresponding to $\Delta pH_{ant} = \Delta pH_{ant}$-TTD is showed with the dashed-dotted grey line.

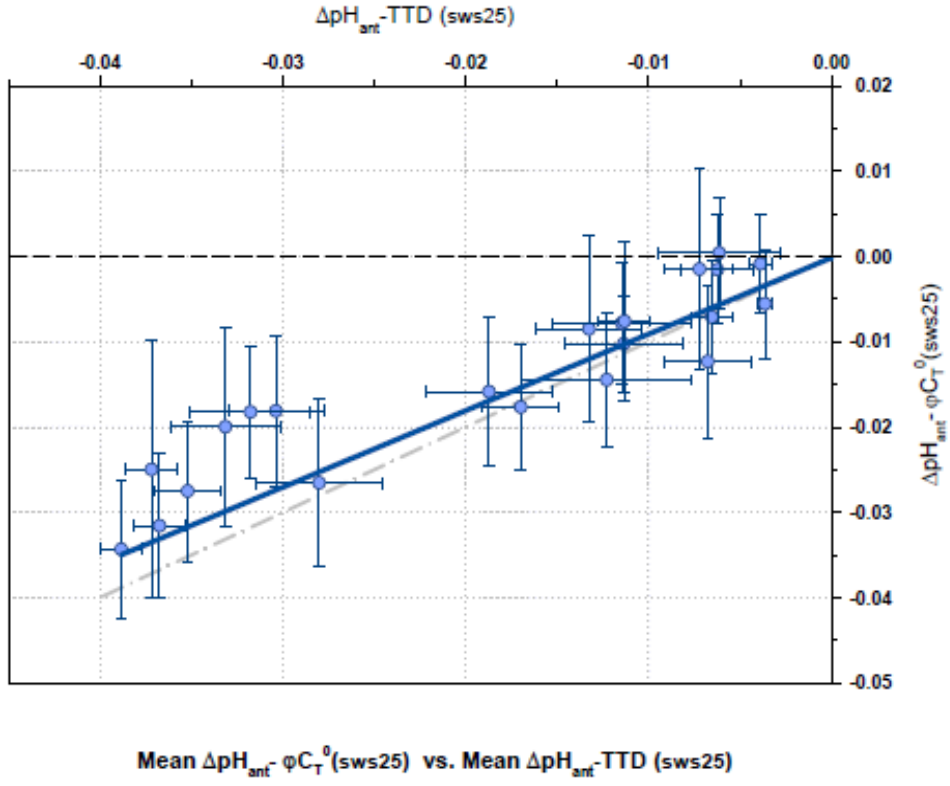

References

Brewer, P. G. (1978), Direct observation of the oceanic CO2 increase, *Geophysical Research Letters*, *5*(12), 997-1000.

Chen, G. T., and F. J. Millero (1979), Gradual increase of oceanic CO2, *Nature*, *277*(5693), 205-206.

Gruber, N., Sarmiento, J.L., Stocker, T.F (1996). An improved method for detecting anthropogenic CO_2 in the oceans, *Global Biogeochemical Cycles*, 10, 809-837.

Khatiwala, S., et al. (2013), Global ocean storage of anthropogenic carbon, *Biogeosciences*, *10*, 2169-2191.

Kortzinger, A., L. Mintrop, and J. C. Duinker (1998), On the penetration of anthropogenic CO2 into the North Atlantic Ocean, *Journal of Geophysical Research C: Oceans*, *103*(C9), 18,681-618,689.

Pérez, F. F., M. Vázquez-Rodríguez, E. Louarn, X. A. Padín, H. Mercier, and A. F. Ríos (2008), Temporal variability of the anthropogenic CO2 storage in the Irminger Sea, *Biogeosciences*, *5*(6), 1669-1679.

Steinfeldt, R., M. Rhein, J. L. Bullister, and T. Tanhua (2009), Inventory changes in anthropogenic carbon from 1997–2003 in the Atlantic Ocean between 20°S and 65°N, *Global Biogeochemical Cycles*, *23*(3), GB3010.

Talley, L. D., G. L. Pickard, W. J. Emery, and J. H. Swift (2011), Chapter 9 - Atlantic Ocean, in *Descriptive Physical Oceanography (Sixth Edition)*, edited, pp. 245-301, Academic Press, Boston.

Tanhua, T., A. Körtzinger, K. Friis, D. W. Waugh, and D. W. R. Wallace (2007), An estimate of anthropogenic CO2 inventory from decadal changes in oceanic carbon content, *Proceedings of the National Academy of Sciences*, *104*(9), 3037-3042.

Tanhua, T., A. Biastoch, A. Körtzinger, H. Lüger, C. Böning, and D. W. R. Wallace (2006), Changes of anthropogenic CO2 and CFCs in the North Atlantic between 1981 and 2004, *Global Biogeochemical Cycles*, *20*(4), GB4017.

Touratier, F., and C. Goyet (2004), Definition, properties, and Atlantic Ocean distribution of the new tracer TrOCA, *Journal of Marine Systems*, *46*(1-4), 169-179.

Touratier, F., L. Azouzi, and C. Goyet (2007), CFC-11, Δ14C and 3H tracers as a means to assess anthropogenic CO2 concentrations in the ocean, *Tellus, Series B: Chemical and Physical Meteorology*, *59*(2), 318-325.

Vázquez-Rodríguez, M., F. Touratier, C. Lo Monaco, D. W. Waugh, X. A. Padin, R. G. J. Bellerby, C. Goyet, N. Metzl, A. F. Ríos, and F. F. Pérez (2009), Anthropogenic carbon distributions in the Atlantic Ocean: data-based estimates from the Arctic to the Antarctic, *Biogeosciences*, *6*(3), 439-451.

Warner, M. J., and R. F. Weiss (1985), Solubilities of chlorofluorocarbons 11 and 12 in water and seawater, *Deep Sea Research Part A. Oceanographic Research Papers*, *32*(12), 1485-1497.

Waugh, D. W., T. W. N. Haine, and T. M. Hall (2004), Transport times and anthropogenic carbon in the subpolar North Atlantic Ocean, *Deep-Sea Research Part I: Oceanographic Research Papers*, *51*(11), 1475-1491.

Waugh, D. W., T. M. Hall, B. I. McNeil, R. Key, and R. J. Matear (2006), Anthropogenic CO2 in the oceans estimated using transit time distributions, *Tellus, Series B: Chemical and Physical Meteorology*, *58*(5), 376-389.